Photosynth Res (2009) 99:115–125
DOI 10.1007/s11120-009-9408-4

REGULAR PAPER

Kinetics of in vivo bacteriochlorophyll fluorescence yield and the state of photosynthetic apparatus of purple bacteria

David Bina · Radek Litvin · Frantisek Vacha

Received: 10 September 2008 / Accepted: 14 January 2009 / Published online: 6 February 2009

Abstract The light-induced electron transport in purple bacterium *Rhodobacter sphaeroides* was studied in vivo by means of kinetic difference absorption spectroscopy and kinetics of bacteriochlorophyll fluorescence yield. Measurements of redox state of the oxidised primary donor and cytochrome *c* and the membrane potential revealed a complex pattern of changes of the electron flow. Effects of the membrane potential on the fluorescence yield were also analysed, and a model for the fluorescence induction curve is presented. The data indicate substantial positive effect of the membrane potential on the fluorescence emission in vivo. Moreover, light-induced changes in light scattering were observed, which suggests occurrence of structural changes on the level of the photosynthetic membrane.

Keywords Photosynthesis · Fluorescence induction · *Rhodobacter sphaeroides* · Membrane potential · Light scattering · Absorbance changes

Abbreviations

A	Absorbance
BChl	Bacteriochlorophyll
FCCP	Carbonylcyanide-p-trifluoromethoxyphenyl hydrazone
LHI, LHII	Light-harvesting complex I, II
P_{870}	Primary donor of the bacterial reaction centre
PSII	Photosystem II
Q_A	First quinone electron acceptor
Q_B	Second quinone electron acceptor
RC	Reaction centre

D. Bina · R. Litvin · F. Vacha (✉)
Biology Centre of AVCR, v.v.i, Institute of Plant Molecular Biology, Branisovska 31, 370 05, Ceske Budejovice, Czech Republic
e-mail: vacha@jcu.cz

D. Bina · R. Litvin · F. Vacha
Faculty of Science, University of South Bohemia, Branisovska 31, 370 05, Ceske Budejovice, Czech Republic

F. Vacha
Institute of Physical Biology, University of South Bohemia, Zamek 136, 373 33, Nove Hrady, Czech Republic

Introduction

Purple nonsulphur bacteria convert light energy into the electrochemical potential through the directional proton translocation connected to a cyclic electron transfer between the reaction centre (RC) and the cytochrome bc_1 complex mediated by mobile carriers cytochrome c_2 and ubiquinone/ubiquinol redox pair (Drews and Golecki 1995). Structural and functional homology between the purple bacterial RC and the RC of the photosystem II (PSII) of the oxygenic photosynthesis allows the use of variable bacteriochlorophyll (BChl) fluorescence to investigate the energy transfer and electron transport within the photosynthetic apparatus in photosynthetic bacteria in a manner similar to plants and algae (Joss et al. 1994; Koblizek et al. 2005; Kolber et al. 2001; Law et al. 1997; Schmidt and Trissl 1998; Strasser and Ghosh 1995; Setlik et al. 1990; Trissl 1996; Trissl et al. 1999).

Primary difference between the two types of RC is that in PSII the fluorescence yield is mainly governed by the redox state of primary electron acceptor (Q_A), while in purple bacteria the fluorescence yield is affected by the redox state of both Q_A and the primary electron donor (P_{870}) (van Grondelle 1985). So far, minor attention has been paid to other factors that influence the energy

transformation in the photosynthetic apparatus and thus the fluorescence yield in bacteria. It was shown that in *Rhodospirillum (Rsp.) rubrum*, phosphorylation of LHI subunits regulates excitonic cooperativity, the efficiency of energy transfer from antenna to the RC and consequently the fluorescence yield (Holmes and Allen 1986; Ghosh et al. 1994). Several researchers have stated that the fluorescence yield in purple bacteria is influenced by the membrane potential. In a study on isolated bacterial photosynthetic membranes (chromatophores) from *Rhodobacter* (*Rb.*) *sphaeroides*, Sherman and Cohen (1972) observed that the light-induced accumulation of protons in the chromatophore lumen was accompanied with increased fluorescence quenching. Electric field-induced fluorescence quenching was also observed to occur directly in isolated light-harvesting complexes (Gottfried et al. 1991). Steiger and Sauer (1995) found that the non-radiative energy dissipation in chromatophores from *Rb. sphaeroides* is affected by the membrane potential with respect to the redox state of the RC. The fluorescence yield was decreased by the electric field at the electroneutral state $P_{870}Q_A$ and charged $P_{870}{}^{+}Q_A^{-}$ state, and increased in the $P_{870}Q_A^{-}$ state. Enhancement of the fluorescence yield was ascribed to the decrease of the rate constant of the charge separation and consequent higher probability of return of the excitation from the primary donor to the antenna. This is supported by results obtained on isolated RCs (Franzen and Stanley 2002; Lao et al. 1993; Popovic et al. 1986; Tanaka and Marcus 1997). On the basis of experimental and theoretical evidence, the primary charge separation (formation of radical pair consisting of oxidised P_{870} and reduced bacteriopheophytin) was identified as the step that is most affected by the electric field (Lao et al. 1995).

In plants, it is well established that the occurrence of the electric field increases the fluorescence yield, most probably by influencing the rate of charge separation (Bulychev et al. 1986; Dau and Sauer 1991; Dau et al. 1991; Pospisil and Dau 2002; Vredenberg 2000; Vredenberg and Bulychev 2002; Vredenberg and Bulychev 2003). However, in the purple bacteria, the exciton-radical pair model established for description of the PSIIRC cannot be applied in a straightforward manner (Bernhardt and Trissl 2000; Amesz and Neerken 2002); hence, the response of the fluorescence yield to the membrane potential in bacteria might differ from oxygenic photosynthesis.

Recent years have seen an increase in interest in the organisation of the electron transport chain of the purple bacteria that goes beyond the structure of single pigment–protein complexes. Functional studies (Comayras et al. 2005a, b; Joliot et al. 1989; Lavergne et al. 1989; Joliot et al. 1997; Jungas et al. 1999; Verméglio and Joliot 2002) demonstrated the importance of the supramolecular structure for the operation of the photosynthetic electron transport. However, the dynamic regulation of the electron transport chain in bacteria has not been investigated in depth so far.

In the present work, we introduce a robust experimental approach that allows monitoring of the electron transport in whole cells of purple bacteria in vivo through measurement of fluorescence yield combined with kinetic absorption spectroscopy. Our aims were (a) characterisation of kinetics of redox changes of major electron-transfer chain components during the adaptation of the photosynthetic apparatus to light; (b) characterisation of membrane potential effect on fluorescence yield in vivo.

Materials and methods

Purple non-sulphur bacterium *Rhodobacter sphaeroides*, strain Y, was grown anaerobically in Sistrom medium (Sistrom 1962) in 25 ml screw top flasks under incandescent lamp, providing irradiance of about 150 μmol m^{-2} s^{-1} on the surface of the cultivation vessel. Cells were harvested after reaching optical density (OD) of 1 at 700 nm, washed with 20 mM K-phosphate buffer of pH 6.8 and resuspended in fresh Sistrom medium to the OD_{700} of 0.2 (6 μmol(BChl) l^{-1} estimated using the procedure of Siefert et al. 1978). Prior to the measurement, the cells were bubbled by nitrogen and placed in a plastic cuvette sealed to keep anaerobic conditions during measurement. Chromatophores were isolated using procedure of de Grooth and Amesz (1977) and resuspended in 50 mM Tris buffer of pH 8 to OD = 0.7 at 850 nm (~7 μmol(BChl) l^{-1}) for measurement.

Parallel measurements of absorbance changes and fluorescence yield were performed using a laboratory-built multichannel kinetic absorption spectrometer described in detail elsewhere (Bina et al. 2006). Fiber-Lite A3200 (Dolan-Jenner, USA) halogen lamp was used as a source of the actinic illumination. Actinic light was filtered with a heat-reflecting interference filter Calflex (Balzers, Switzerland) and switched by a shutter with opening halftime of 0.5 ms (Uniblitz VMD-D1, Vincent Associates, USA). Actinic light as well as the measuring pulses for fluorescence were delivered to the sample by a fibre optics bundle through a blue filter, Corning 4–96. The irradiance provided by the actinic lamp was up to 2,000 μmol m^{-2} s^{-1} on a surface of the sample cuvette. Single-turnover actinic flashes (energy 4 mJ) were produced by a xenon lamp FX-249 (E.G&G, USA) and filtered by Corning 4–96 filter. Bacteriochlorophyll fluorescence was usually measured using 2 μs pulses emitted by sets of light emitting diodes (LEDs) with emission maxima 460 nm. Diodes emitting at 850 or 890 nm were used in some cases as indicated below. Total fluorescence emission above 750 nm was detected.

Results and discussion

Overview of light-induced absorbance changes in whole cells of *Rb. sphaeroides*

Illumination of whole cells and chromatophores of wild-type *Rb. sphaeroides* produces well-known characteristic absorbance changes in the visible and near infrared region of the absorption spectrum. We present a brief overview of the changes observed in our samples. The difference absorption spectra are shown in Fig. 1, for comparison refer to e.g. de Grooth and Amesz (1977). The most pronounced features are the electrochromic shift of absorption bands of carotenoids at 480–530 nm and bacteriochlorophyll of the light-harvesting complex II (LHII) around 850 nm (these are frequently used as linear indicators of the membrane potential e.g. Jackson and Crofts 1969) and the bleaching of bands of the primary donor around 870 nm (Q_y band) and 600 nm (Q_x band). The oxidation of the primary donor (P_{870}) can also be detected indirectly, by the electrochromic shift of the absorption band of the accessory BChl centred at 800 nm (Okamura et al. 1982). Besides, the redox state of *c*-type cytochromes can be monitored using the extent of bleaching of the band around 553 nm (Cotton and Jackson 1982).

In Fig. 1a, we present the difference spectra obtained 3 μs (full circles) and 20 ms (empty circles) after a single-turnover flash. In the spectrum measured at 3 μs, bleaching of peaks around 600 and 870 nm indicates oxidation of primary donor BChl. The derivative-shaped feature around 800 nm arises from the shift of the accessory BChl band in presence of P_{870}^+. Also present in the spectrum are the electrochromic shifts of carotenoids (480–530 nm) and the LHII antenna-bound BChl around 850 nm. Within 3 μs after the flash, the shifts are mostly due to the presence of P_{870}^+ rather than to the membrane potential resulting from proton translocation. In the 20 ms spectrum, all features connected to P_{870}^+ are significantly diminished, signalling the reduction of P_{870}^+. The spectrum is dominated by electrochromic shift of carotenoid (480–530 nm) and antenna BChl (around 850 nm) absorption bands. Since P_{870}^+ has already disappeared, the electrochromic shift now indicates the build up of the membrane potential due to the operation of cytochrome. This will be illustrated later in the section dedicated to kinetics of absorbance changes.

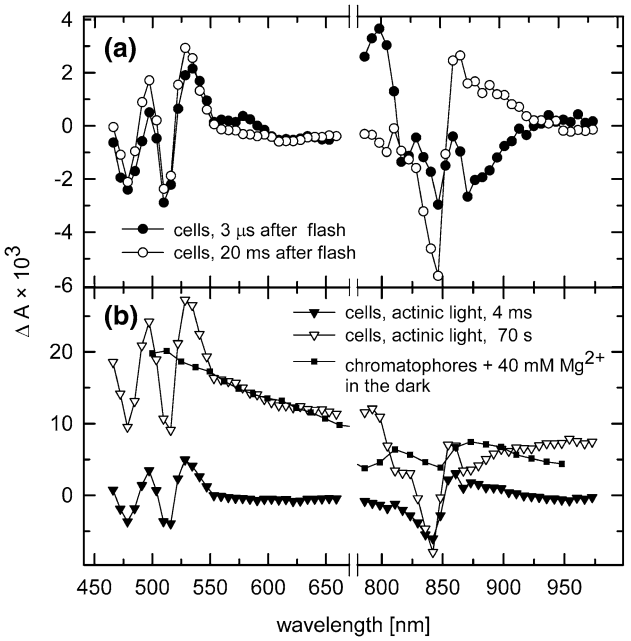

Fig. 1 **a** Flash-induced absorbance difference spectra in whole cells of *Rb. sphaeroides*, 3 μs (–●–) and 20 ms (–○–) after a single turnover (2 μs) flash. **b** Absorbance changes induced by continuous actinic illumination in whole cells, after 4 ms (–▼–) and 70 s (–▽–) of actinic light and an ion-induced absorbance change in chromatophores in the dark (–■–)

Absorbance changes appearing during continuous illumination, shown in Fig. 1b, correspond to the flash-induced ones. However, during the course of illumination, the spectra become distorted by an upward baseline shift apparent over the whole spectrum [compare spectra measured after 4 ms (full triangles) and 70 s (empty triangles) after the onset of actinic illumination]. This feature appeared consistently in all measurements done with the continuous actinic illumination. Its wavelength dependence suggests that the origin of this phenomenon lies in an increase of light scattering. Treatment of the cells with atrazine (blocks Q_B pocket) and uncouplers (ionophores FCCP and gramicidin) prevented its appearance, indicating dependence on functional photosynthetic electron transport and selective membrane permeability to ions. We also observed similar changes in cells of species *Rsp. rubrum* and *Rubrivivax gelatinosus*. In chromatophores, increase of scattering was never observed under illumination, not even in presence of artificial electron donors, but a very similar signal could be brought about in the dark by addition of Mg^{2+} or Ca^{2+} in millimolar concentrations (Fig. 1b, squares). This bivalent cation-induced scattering was also observed in whole cells in the dark. Monovalent cations, such as K^+, were ineffective in inducing the scattering irrespective of their concentration in both whole cells and chromatophores. Since Varga and Staehelin (1985) observed Mg^{2+}-induced lateral aggregation of light harvesting complexes from *Rhodopseudomonas palustris* in liposomes, the scattering observed in our experiments might be brought about by a conformational change of the plasmatic membrane caused by ion-induced reorganisation of pigment–protein complexes. On the other hand, structural studies indicate dense packing of pigment–protein complexes in the photosynthetic membrane of purple bacteria (e.g. Sturgis and Niederman 2008) which seems to

limit the possibility of lateral movement of components of photosynthetic apparatus.

Alternative explanation of the structural changes that cause the increase of the light scattering is the swelling of the invaginations of the plasmatic membrane due to local changes in local ion concentrations. This, however, does not seem to be supported by observations of bivalent cation-induced scattering in the dark, especially in chromatophores. Clearly, more experimental work is needed to clarify the background of the light-scattering changes in purple bacteria.

Kinetics of absorbance changes

Flash-induced changes

We have monitored the kinetics of the absorbance changes with respect to primary donor P_{870} and cytochrome *c* oxidation and changes in membrane potential. Traces in Fig. 2 show the decay of P_{870}^+ (ΔA_{798}, full triangles), paralleled by the cytochrome *c* oxidation ($\Delta A_{570} - \Delta A_{553}$, crosses) and the subsequent reduction of the cytochrome and the build-up of the membrane potential (indicated by the electrochromic shift, $-\Delta A_{840}$, empty triangles) through the operation of the cytochrome bc_1 complex (Cotton and Jackson 1982; Mulkidjanian and Junge 1994). To facilitate orientation in the figure, we plotted also the least-square fits of the kinetic traces (biexponential decay for P_{870}^+, monoexponential rise and decay for cytochrome *c*, biexponential rise followed by a monoexponential decay for the membrane potential). Since these serve just as a guide, they will not be discussed further. We preferred the amplitude of the electrochromic shift around 800 nm to the bleaching of primary donor Q_x band around 600 nm as the indicator of P_{870} oxidation in single flash experiments, because the amplitude of the former change was larger, resulting in higher signal to noise ratio. Moreover, in single flash experiments, the maximal build up of the membrane potential occurs only after P_{870}^+ has decayed thus a distortion of the signal at 800 nm by the shift of LHII-B850 band at 850 nm has minimal effect on analysis of P_{870}^+ decay. However, for the continuous-light experiments, where large electrochromic signals of antenna BChl emerge along with P_{870}^+, the 600 nm (Q_x) band was more useful for P_{870}^+ detection.

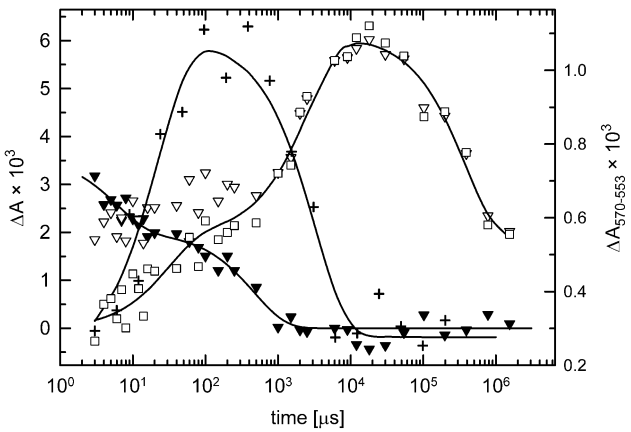

Fig. 2 Kinetics of flash-induced absorbance changes in whole cells of *Rb. sphaeroides*. Data from a single shot measurement are presented to illustrate the signal to noise ratio of our instrument setup. Kinetics correspond to the decay of oxidised primary donor (ΔA_{798}, ▼), oxidation and reduction of cytochrome *c* ($\Delta A_{570-553}$, +, right Y-axis) and the build up of the membrane potential detected by the electrochromic shift of BChl ($-\Delta A_{840}$, ∇). Trace marked by empty squares (□) represents the kinetics of membrane potential corrected for the contribution of oxidised primary donor, as described in the text. Smooth lines were obtained by fitting of the kinetic traces by a sum of exponentials

The electrochromic kinetic traces had to be corrected for the effect of charge of P_{870}^+ to obtain the information on the proton translocation-induced membrane potential. We assumed that the experimentally observed electrochromic shift can be with reasonable accuracy taken for a sum of a component related to the proton translocation and a component proportional to the amount of P_{870}^+. Thus, we subtracted the trace of P_{870}^+ multiplied by the ratio of amplitudes of the absorbance change corresponding to P_{870}^+ and the electrochromic signal measured 3 μs after the flash. The correction assumes that immediately after a single-turnover flash, the electrochromic change is due solely to P_{870}^+. Applied to the infrared bands, this means that the correct kinetics of membrane potential, *S*, follows the relation: $S = (-\Delta A_{840}) - \Delta A_{798} \cdot q$, where $q = -\Delta A_{840}(\text{flash})/\Delta A_{798}(\text{flash})$ is the ratio of amplitudes of the flash-induced changes (at 3 μs after the flash). Since ΔA_{840} is the amplitude of the negative peak of the signal due to the electrochromic shift of the antenna BChl (cf. Fig. 1) and ΔA_{798} is proportional to the amount of P_{870}^+, *q* corresponds to the electrochromic shift per unit of P_{870}^+ (measured as the absorbance change). Consequently, for the kinetic trace, $\Delta A_{798} \cdot q$ corresponds to the component of the of the electrochromic shift elicited by P_{870}^+ alone. Analogous computation can be done using absorbances of appropriate bands in the visible region. In Fig. 2, the corrected trace is denoted by squares. The same correction using the flash-induced features was applied also to continuous illumination-induced kinetics described in the following section.

Continuous light

Figure 3a presents kinetics of absorbance changes under a continuous illumination of 2,000 μmol m^{-2} s^{-1}. In this case, presence of scattering requires that baseline of the spectra is corrected prior to extraction of kinetic data. This

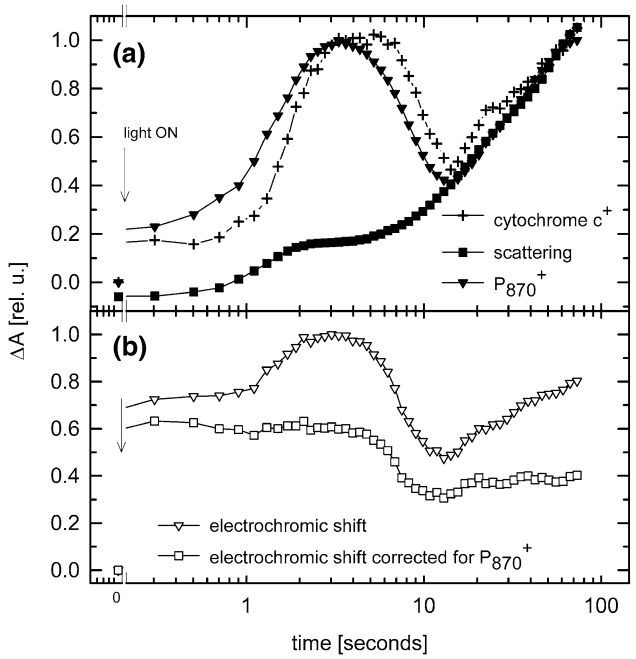

Fig. 3 Kinetics of absorbance changes in whole cells of *Rb. sphaeroides* during continuous illumination of 2,000 μmol m^{-2} s^{-1}. **a** –▼– oxidised primary donor ($-\Delta A_{602}$), – + – oxidised cytochrome *c*, –■–, kinetics of increase of the light scattering, detected as amplitude of baseline shift of difference spectra at 660 nm. Kinetics of scattering was normalised to match the rising part of the kinetics of P_{870}^+ after 15 s. **b** –▽– kinetics of the membrane potential, detected by the electrochromic shift of carotenoids ($\Delta A_{503} - \Delta A_{480}$), –□– the same kinetics after correction for primary donor contribution

was done by subtracting a linear function passing through the spectra at 580 and 660 nm. Positions of peaks of the corrected spectra corresponded well to the available data (e.g. de Grooth and Amesz 1977); thus we assumed that the linear correction is sufficiently accurate. The traces correspond to changes of the amount of oxidised primary donor ($-\Delta A_{602}$, full triangles), oxidised cytochrome *c* ($\Delta A_{570} - \Delta A_{553}$, crosses) and changes in light-scattering, i.e. extend of the baseline shift measured in the region, where changes of absorbance are minimal (ΔA_{660}, full squares; this value had to be extracted prior to baseline correction). After opening of the shutter, oxidation of the primary donor proceeded through an intermediate step at about 0.4 s to a peak at 3 s. Position of this peak varied among preparations from different cultures by about 2 s. This peak was followed by a minimum at about 15 s, from where the amount of oxidised primary donor slowly rose to a steady state, reached usually within 80 s. Position of this minimum was in some samples shifted to longer times (by a maximum of 5 s).

Kinetics of the cytochrome *c* oxidation was similar to P_{870}^+; however, the phases occurring up to 15 s were slightly (by about 1 s) shifted to later times. Starting from the minimum at 15 s, the oxidation of cytochrome preceded oxidation of the primary donor.

The amplitude of the baseline shift due to scattering rose usually in two phases. First was complete in about 3 s. The second, slower, phase of the increase led to a steady state, which was reached in times over 70 s after the onset of actinic illumination (not shown in the graph).

Figure 3b shows both the "raw" kinetic trace of the electrochromic shift ($\Delta A_{503} - \Delta A_{480}$, triangles), and the trace corrected for P_{870}^+ (squares). Kinetics of the electrochromic shift was similar to the course of P_{870}^+ signal in Fig. 3a with a fast rise and a peak at around 3–6 s. The initial increase (<1 s) was, however, faster than that of P_{870}^+. The correction for P_{870}^+ (amounts to about 40% of the total electrochromic signal), reduces significantly the amplitude of the peak at 3 s and also diminishes the increase that starts in 15 s. The corrected trace suggests that the value of the membrane potential stabilised in about 20 s.

The decay of absorbance changes in the dark was mostly complete within 1 s except for the scattering, which disappeared only after several minutes in the dark (not shown). Both the electrochromic signal and scattering kinetics measured during illumination in bacteria bear striking resemblance to kinetics obtained in plant chloroplasts (see Kramer and Sacksteder 1998).

When the kinetic measurements were performed under different actinic irradiances, it was found that the extent of the primary donor oxidation decreased by only 10% upon lowering of the irradiance to 1,200 μmol m^{-2} s^{-1}. When the irradiance decreased to 150 μmol m^{-2} s^{-1}, maximum P_{870} oxidation decreased about threefold. Times at which the phases of the kinetics appeared were not significantly affected by the change in irradiance. After further decrease to 50 μmol m^{-2} s^{-1}, however, almost none recognisable peak remained in the kinetics. In order to estimate the amount of RCs that remained open during continuous illumination, single turnover flashes were added. We found that at 2,000 μmol m^{-2} s^{-1}, the flash increased the amount of oxidised primary donor by less than 5% during the maximum and by about 10%, in the late, (>30 s) phase of the induction curve (not shown). Thus under strong irradiance, majority of the RCs are in either P_{870}^+ or $P_{870}Q_A^-$ state, consequently, the observed drop of P_{870}^+ at 10 s is not due to opening of the RCs but due to an increase of $P_{870}Q_A^-$ relative to P_{870}^+.

The amount of oxidised primary donors is determined by the ratio between electron flows on donor and acceptor sides of the RC, i.e. from cytochrome c_2 to P_{870}^+ and from the RC to the ubiqinone pool. Initial increase of P_{870}^+ (0–4 s in Fig. 3a) reflects electrons being transferred to ubiquinones. Then the reduction of P_{870}^+ by the cytochrome c_2 prevails and the amount of P_{870}^+ decreases (4–15 s in Fig. 3a), being replaced by $P_{870}Q_A^-$. This may indicate reduction of the ubiquinone pool available in the vicinity of RCs. The slow increase of P_{870}^+, which follows

after the minimum at 15 s, suggests a relative increase of the electron flow on the acceptor side of the RC, towards the cytochrome bc_1 complex. If the membrane ubiquinone pool was close to full reduction in the anaerobic conditions prior to the illumination (Joliot et al. 2005), it could be assumed that it is fully reduced during the initial stages of illumination. Consequently, the slow increase of P_{870}^+ could indicate an increased rate of diffusion of the ubiquinone. However, according to recent work (Grammel and Ghosh 2008) the proportion of reduced ubiquinone does not exceed about 70% under redox conditions corresponding to photosynthetic growth. In that case the observed change indicates probably the slow equilibration among different parts of membrane ubiqinone pool.

Interestingly, the changes of light-scattering occur on the same time scale as the increase of P_{870}^+ in times longer that 15 s. This is illustrated in Fig. 3a, where kinetics P_{870}^+ and light scattering are presented together, normalised to match at times longer than 15 s to stress the parallel trends. This suggests a connection between the structural changes of the membrane and the photosynthetic electron flows. However, more experimental work is needed to establish concrete explanations for these processes.

Analysis of fluorescence induction curves

Characteristics of fluorescence induction curves

Figure 4 shows examples of fluorescence induction curves on whole cells measured under high irradiance, 2,000 μmol m^{-2} s^{-1} (full circles) and moderate irradiance, 150 μmol m^{-2} s^{-1} (empty circles). After a fast initial increase which appears as a single step in our measurements due to the low time resolution (in fact, it consists of several sub-phases Strasser and Ghosh 1995) the fluorescence induction curve typically exhibits a peak at 2 s with a shoulder around 5 s. In the kinetics measured at lower irradiance, there is also a prominent peak at about 15 s, which is occasionally observed in kinetics measured at high irradiance as a shoulder. As has been already noted (e.g. Setlik et al. 1990; Strasser and Ghosh 1995), fluorescence induction curves in purple bacteria are remarkably similar to oxygenic photosynthesis as can be readily seen in the inset of Fig. 4, where we present a fluorescence induction curve measured on Norway spruce needles. This trace was measured using the commercial PAM-2000 fluorimeter (Walz, Germany) under irradiance 120 μmol m^{-2} s^{-1}.

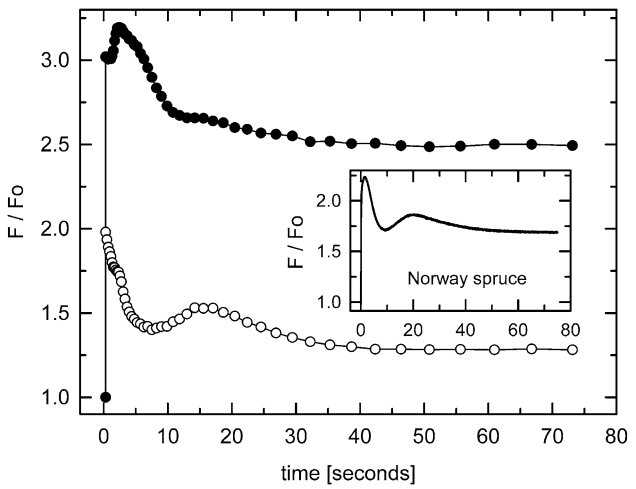

Fig. 4 Fluorescence induction curves measured on whole cells of *Rb. sphaeroides* under 2,000 μmol m^{-2} s^{-1} (–●–) and 150 μmol m^{-2} s^{-1} (–○–). Inset: fluorescence induction curve measured on needles of Norway spruce (*Picea abies*) under 120 μmol m^{-2} s^{-1}

Correspondence of fluorescence induction curves and absorbance changes

Comparison of Figs. 3 and 4 immediately shows marked differences between fluorescence induction curves and kinetics of P_{870}^+ (kinetics of P_{870}^+ at high and moderate irradiance were qualitatively similar thus the presented P_{870}^+ kinetics can be used as reference for both irradiances). This is more remarkable for the high irradiance case, since, as argued above, at 2,000 μmol m^{-2} s^{-1}, almost all RCs are either in P_{870}^+ or in $P_{870}Q_A^-$ state. The P_{870}^+ state of the RC is the one with the highest fluorescence yield, $F_M(P_{870}^+)/F_o \approx 3.5$ while for the $P_{870}Q_A^-$ state $F_M(P_{870}Q_A^-)/F_o \approx 2$ (e.g. Koblizek et al. 2005; Kingma et al. 1983), F_o denotes the fluorescence of open RCs, i.e. the $P_{870}Q_A$ state. Consequently, in this two-state case, one would expect the overall shape of the induction curve to follow the course of P_{870}^+, which is not the case. A peak around 3 s was indeed present in the fluorescence induction curve at 2,000 μmol m^{-2} s^{-1}, at 150 μmol m^{-2} s^{-1} there was a shoulder. However, as noted above, in the fluorescence induction curve the structure of this peak was more complex than in absorbance, therefore the correspondence of these features is not straightforward. This peak was not followed by a minimum around 15 s. Instead, another peak appeared at this time. This feature was more prominent in the fluorescence induction curves measured at moderate irradiance. Due to the fact that P_{870}^+ is at minimum at these times, this peak probably indicates accumulation of $P_{870}Q_A^-$. This peak was followed by a slow decrease that led to a steady state beyond 50 s, while a parallel increase of the amount of P_{870}^+ took place. All these discrepancies suggest that fluorescence induction curves cannot be interpreted only in terms of changes of concentrations of redox states of RCs.

Effect of the membrane potential upon the fluorescence yield

In the following section, we will focus on the possible contribution of changes of the membrane potential to the modulation of BChl fluorescence yield with respect to different redox states of RC. First, simpler cases of samples with only one predominant redox state of RC will be presented; later we will proceed to analysis of classical fluorescence induction curves.

Open reaction centres To study the effect of the membrane potential upon the fluorescence emission of open RCs, we utilised 2 μs single-turnover flashes arranged in series of 37. Flashes were spaced by 50 ms. We found that this approach allowed accumulation of the membrane potential, while keeping the amount of both P_{870}^{+} and Q_A^- low. Moreover, no increase of light scattering was observed in these experiments. The experiments were done both on untreated samples and in the presence of uncouplers, such as FCCP or gramicidin. Results are shown in Fig. 5. The start and the end of the flash series are denoted by arrows. The flashes brought about twofold increase of the fluorescence yield due to oxidation of P_{870} and reduction of Q_A^-. The first point of the measurement in Fig. 5 was done 30 ms after the last flash. By this time, the fluorescence yield had already decayed significantly. In the presence of uncouplers, the decay led to a value equal to F_o (open circles). In the difference spectra, no signal corresponding to either P_{870}^{+} or electrochromic shift was present after 1 s after the last flash (not shown). In untreated samples, a pronounced dip by about 10% appeared at the beginning followed by slow recovery to F_o value in about 250 s (closed circles). This was paralleled by the decay of membrane potential-sensing electrochromic signals. Again, signals pertinent to P_{870}^{+} disappeared within 1 s after the last flash. Difference spectra then corresponded to those denoted by open symbols in Fig. 1a, i.e. dominated by slowly decaying electrochromic absorbance changes. As shown in the inset of Fig. 5, a linear relationship between the membrane potential (expressed by the amplitude of the electrochromic absorbance changes) and the decrease of fluorescence yield was observed, in other words, the sample exhibited a membrane potential-induced fluorescence quenching, namely, quenching of F_o. To decide whether the quenching occurs in the external antenna, LHII, or in the core complex (RC-LHI), we probed the fluorescence using subsequently excitation to carotenoids (460 nm), BChl of LHII (850 nm) and RC-LHI (890 nm). The same relative decrease of the fluorescence yield after the series of flashes was observed, irrespective of the probe wavelength; thus the quenching most probably occurs in the last step of the excitation transfer chain i.e. the core complex, RC-LHI. Within the core complex, the quenching can be localised in the LHI or in the RC. If the process takes place within the LHI complex, then it can be viewed as competing with the excitation trapping in the RC. Thus one can suppose that the quenching will manifest more strongly in the presence of closed RC, because both P_{870}^{+} and Q_A^- lead to decreased excitation trapping efficiency, thus the flow of excitation energy through the quenching channel will increase relatively. On the other hand, one would expect that if the quenching is located in the RC, it would be diminished by the oxidation of the primary donor. We modified the above described experiment to include additional excitation flashes fired after the end of the actinic flash series, in times when the quenching appears. These flashes were spaced at least by tens of seconds to ensure that their integral actinic effect was negligible. The fluorescence yield was monitored closely after the flashes. We did not observe indications of increased fluorescence quenching at 3 μs after the flash, thus in presence of P_{870}^{+} nor at 400 μs, mostly in the $P_{870}Q_A^-$ state (not shown). We thus conclude that the quenching most probably reflects enhanced non-radiative dissipation in the RC (Franzen and Stanley 2002).

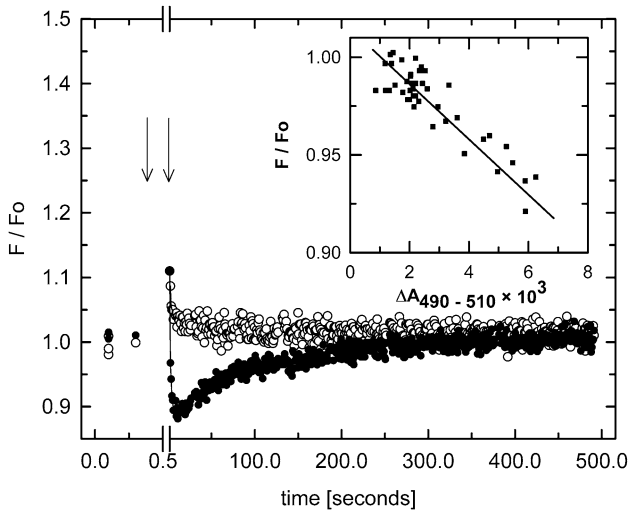

Fig. 5 Kinetics of fluorescence measured in the dark after a series of 37 single-turnover (duration 2 μs) flashes spaced 50 ms. Data of control (untreated, ●) and FCCP-treated (○) cells of *Rb. sphaeroides*. Arrows denote start and end of the series of flashes. Fluorescence was probed using LED-pulses with maximum at 460 nm. Inset: normalised fluorescence yield plotted against the electrochromic absorbance change of carotenoids ($\Delta A_{503} - \Delta A_{480}$), i.e. the membrane potential (■), measured in the same experiment; line denotes the best fit of the points by a linear function

Effect of Q_A reduction Further we present a more detailed treatment of membrane potential effect on RC closed by the reduction of the Q_A, because in chromatophores and also in plant chloroplasts, fluorescence yield in presence of Q_A^- was reported to be enhanced by external electric fields

(Bulychev et al. 1986; Dau and Sauer 1991; Dau et al. 1991; Steiger and Sauer 1995; Vredenberg 2000; Pospisil and Dau 2002; Vredenberg and Bulychev 2002; Vredenberg and Bulychev 2003). We studied this effect in whole cells under continuous illumination in the presence of 10 mM sodium dithionite. This treatment decreased the P_{870}^{+} formation and enhanced Q_A^- accumulation. We found that the absorbance changes in the carotenoid and bacteriochlorophyll regions corresponded to the electrochromic signal of untreated cells, without any new features appearing. We thus assumed that no factors other than Q_A reduction and the membrane potential had to be taken into account. During the course of illumination, we observed a correlation of the fluorescence yield and the membrane potential, as shown in Fig. 6, where the fluorescence yield is plotted against the amplitude of the electrochromic absorbance change ($\Delta A_{503} - \Delta A_{480}$). The kinetic traces are plotted in the inset. The graphs contain data from two subsequent runs separated by 15 min of dark. The addition of FCCP to the samples eliminated all electrochromic signals and led to a constant fluorescence yield (F(dithionite + FCCP)/F_o(FCCP) $\sim$ 2.5) during the actinic illumination (not shown). For the purpose of the quantitative analysis of the membrane potential effect, we used a simple model, in which the membrane potential acts against the charge separation in the RC; hence, it increases the probability of return of excitation from RC to the antenna, resulting in enhanced fluorescence emission. We describe the effect by a change of the apparent rate constant of excitation trapping in the $P_{870}Q_A^-$ state, k_{A-}. The fluorescence yield in $P_{870}Q_A^-$ state in the absence of the membrane potential can be expressed as follows:

$$\frac{F\left(P_{870}Q_A^-\right)}{F_o} = \frac{k_o + k_L}{k_L + k_{A-}} \tag{1}$$

where k_o stands for the apparent rate constant of excitation trapping by the open RC, k_L is the rate constant of energy dissipation. It includes both radiative and nonradiative dissipation. In presence of the membrane potential $\Delta\phi$ [mV] we use following approximation of the potential dependence, using the fact that electrochromic shift is linearly dependent on membrane potential:

$$\frac{F\left(P_{870}Q_A^-, \Delta\varphi\right)}{F_o} = \frac{k_o + k_L}{k_L + k_{A-} + k_S \cdot S} \tag{2}$$

$S = \Delta A_{503} - \Delta A_{480}$. The term $k_{A-} + k_S \cdot S$ corresponds to overall decrease of the apparent rate of the charge separation in $P_{870}Q_A^-$ state due to the membrane potential. This effect is in the first approximation assumed to be linear. Equation 2 was used to least-square fit the data using values $k_L = 1/(700\ \text{ps})$ and $k_o = 1/(60\ \text{ps})$, taken from the work of Trissl (1996) and Bernhardt and Trissl (2000). The fit is plotted in the main panel of Fig. 6 (line). It shows that changes of fluorescence yield under reducing conditions can be quantitatively explained by decrease of the apparent rate constant of charge separation due to the external electric field. Experiments repeated on various cell cultures produced average k_{A-} value of 1/(200 ps), corresponding to $F(P_{870}Q_A^-)/F_o \approx 2.8$, with 25% relative decrease of this value due to membrane potential ($k_S \cdot S_{max}/k_{A-} = -0.25$). If one assumes that the maximal membrane potential reached is about 150 mV, this yields about 1.5% change of $F(P_{870}Q_A^-)/F_o$ per 10 mV, which corresponds exactly to value given for chromatophores by Steiger and Sauer (1995). As for the rather high $F(P_{870}Q_A^-)/F_o$ value, we refer to works of Holmes and Allen (1986) and Ghosh et al. (1994), who, after subjecting bacterial samples to low redox potential, observed significantly decreased phosphorylation of the antenna complexes, which brought about an increase of the fluorescence yield. Thus, one would expect that in untreated samples, the k_{A-} value computed using the above-described approach would be higher. This was indeed the case, as will be shown below. Another way to obtain the $F(P_{870}Q_A^-)/F_o$ ratio is to block the Q_B pocket with atrazine, and measure the fluorescence under moderate light intensity, so that the P_{870}^{+} reduction by the cytochrome is fast enough to prevent its accumulation, which can be tested by absorption. Typical value of the $F(P_{870}Q_A^-)/F_o$ ratio at these conditions was about 2.2, which is indeed lower that under presence of dithionite and

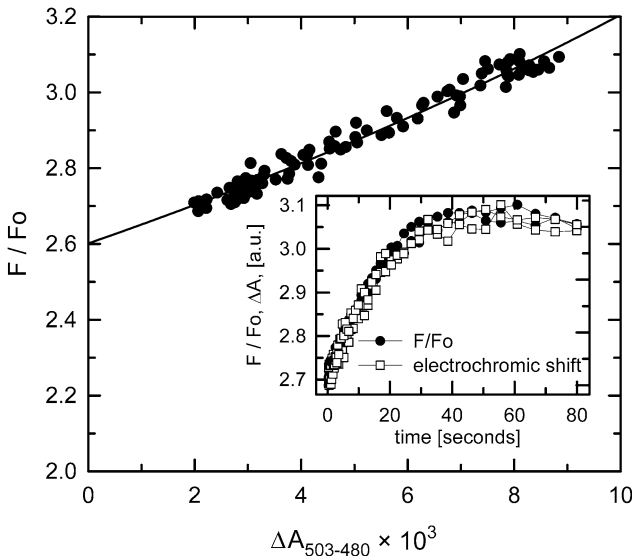

Fig. 6 Dependence of the fluorescence yield on the membrane potential during continuous illumination (2,000 μmol m^{-2} s^{-1}) in dithionite (10 mM) treated sample of cells of *Rb. sphaeroides*. Membrane potential was detected using electrochromic shift of carotenoids ($\Delta A_{503} - \Delta A_{480}$). Line represents the best fit of the data using Eq. 2 described in the text. Inset: kinetics of membrane potential ($\Delta A_{503} - \Delta A_{480}$, –□–) and fluorescence (–●–) during the course of actinic illumination. Data from two subsequent runs, separated by 15 min of dark

also closer to values usually reported in the literature (Koblizek et al. 2005; Kingma et al. 1983; Trissl 1996; Bernhardt and Trissl 2000; van Grondelle 1985; van Grondelle et al. 1994).

Modelling of fluorescence induction curves at high-irradiance Now we will extend our analysis to the fluorescence induction curves measured on untreated samples under continuous illumination. From the above-presented results, it follows that under irradiance so high that full closure of RC could be assumed ($[P_{870}^+]_{rel} + [Q_A^-]_{rel} = [P_{870}^+]/[RC] + [Q_A^-]/[RC] = 1$) the dominant effect of membrane potential should be the increase of the fluorescence yield. First, we define the relative fluorescence yield in the absence of the membrane potential:

$$\frac{F}{F_o} = \frac{k_o + k_L}{k_L + k_{A-} \cdot \left(1 - \left[P_{870}^+\right]_{rel}\right) + k_P \cdot \left[P_{870}^+\right]_{rel}} \quad (3a)$$

Introducing the membrane potential effect in the manner used in Eq. 2 we get:

$$\frac{F}{F_o} = \frac{k_o + k_L}{k_L + (k_{A-} + k_S \cdot S) \cdot \left(1 - \left[P_{870}^+\right]_{rel}\right) + k_P \cdot \left[P_{870}^+\right]_{rel}} \quad (3b)$$

and by rearranging

$$\frac{F}{F_o} = \frac{k_o + k_L}{k_L + k_{A-} + (k_P - k_{A-}) \cdot \left[P_{870}^+\right]_{rel} + k_S \cdot S - k_S \cdot S \cdot \left[P_{870}^+\right]_{rel}} \quad (3c)$$

Then, using the absorbance change pertinent to P_{870}^+ oxidation, such as $-\Delta A_{602}$, can be Eq. 3c rewritten formally as:

$$\frac{F}{F_o} = \frac{k_o + k_L}{k_L + k_1 + k_2 \cdot P + k_3 \cdot S - k_4 \cdot S \cdot P} \quad (4)$$

where $P = -\Delta A_{602}/(-\Delta A_{602})_{max} = [P_{870}^+]/[P_{870}^+]_{max}$, i.e. the kinetics of the absorbance change originating from oxidation of the primary donor normalised to maximum. S corresponds to the kinetics of the electrochromic shift, corrected for the P_{870}^+ contribution. We used Eq. 4 to fit the fluorescence induction curves using Levenberg–Marquardt algorithm to obtain values of constants k_1–k_4. No a priori constraints were applied to the expected values of these rate constants. Figure 7a shows an example of fit results (line) of a fluorescence induction curve (circles). In the inset of the figure, we present a fit of the same data obtained without considering the membrane potential effect (Eq. 3a), i.e. fluorescence yield determined solely by the amount of different redox states of RC. This approach is clearly inadequate. In total, we applied the fit to kinetics measured on 25 different samples The average value of k_1, corresponding to k_{A-} was 1/(138 ps), corresponding to $F(P_{870}Q_A^-)/F_o \approx 2$, in agreement with literature (Kingma et al. 1983). The value ranged between 1/(90 ps) and 1/(190 ps) among samples (i.e. $F(P_{870}Q_A^-)/F_o \approx 1.4$ and 2.7, respectively). The maximum relative decrease of k_{A-} (i.e. $k_3 \cdot S_{max}/k_1$) was 0.49 (ranging from 0.22 to 0.68). This means that compared to dithionite-treated samples, the estimated increase of fluorescence due to Q_A reduction was smaller. At the same time, the overall apparent effect of the membrane potential was about two times larger, both absolutely and relatively. Rate constant k_P can be computed from the fit coefficients as $k_2 \cdot k_3/k_4 + k_1$. This produced an average value 1/(277 ps) [ranging from 1/(200 ps) to 1/(360 ps)] corresponding to $F(P_{870}^+)/F_o \approx 3.6$ (ranging from 2.8 to 4.3). The rate constants computed from the fit were thus reasonably close to values available in literature (Koblizek et al. 2005; Kingma et al. 1983; Trissl 1996; Bernhardt and Trissl 2000; van Grondelle 1985; van Grondelle et al. 1994). In Fig. 7b we present a plot of residuals versus time for all the fits of induction curves. The residuals shown are relative, i.e. divided by respective values of fluorescence yield. It shows that the overall quality of the fits was very good, with most residuals lying within the 5% of the fitted fluorescence values. However, closer inspection also reveals a trend in the distribution of residuals, which is best

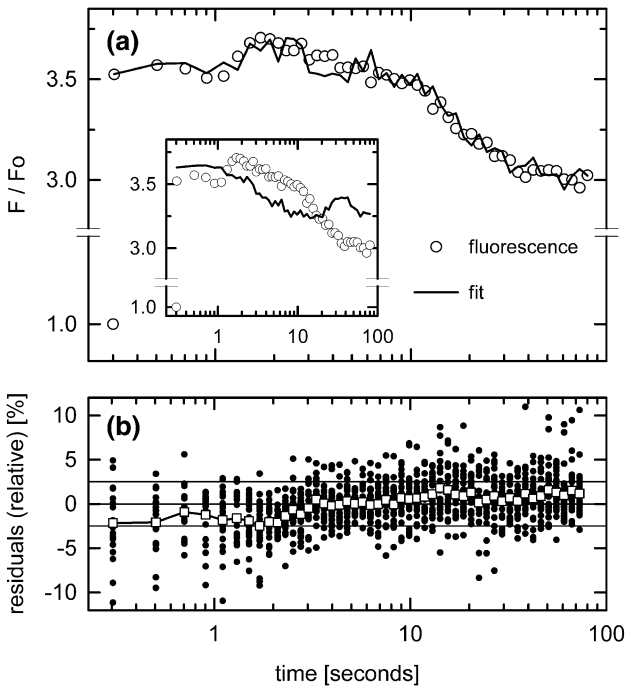

Fig. 7 **a** Fit (line) of the fluorescence induction curve (○) using kinetics of absorbance changes corresponding to the oxidised primary donor and the membrane potential (measured as the electrochromic shift) as described in the text. Inset: Fit of the same data but without considering the membrane potential effect. **b** Plot of residuals of 25 fits of induction curves [including the one in graph (**a**)], using both primary donor and membrane potential. Squares denote the average. Residuals are expressed as percents of corresponding fluorescence values

appreciated from the averaged value of residuals, plotted in squares in Fig. 7b. It is clear that in the early part (up to about 2 s) of the induction curve, most fits tend to predict lower value of fluorescence yield than actually measured, while in the later part, higher yield was predicted. These discrepancies could be due to the simplicity of the mathematical treatment chosen leading to the oversimplification of the description of the physical principles the electric field effect upon reactions within the RC. Moreover, as we report above, certain amount of open RCs is present during course of illumination, mainly in the later phases of the induction, which is not taken into account in our model. Presence of these open centres could cause a lowering of fluorescence yield compared to our model. This effect of open centres would be enhanced also by the membrane potential-induced fluorescence quenching. Despite these reservations, our model in its simplicity clearly offers a reasonably accurate approximation of the fluorescence induction curves measured under high irradiance while supporting the idea of modulation of the fluorescence yield in purple bacteria by the membrane potential.

Conclusions

Present data support the interpretation that the fluorescence yield in purple bacteria in vivo is significantly modulated by the membrane potential; thus changes of fluorescence alone are not sufficient to yield information on the electron flow in the membrane, especially on the amount of P_{870}^{+}. We have also shown that measurements of P_{870} and cytochrome *c* oxidation uncover complex changes of the electron flow that could not be judged from the fluorescence yield changes only. In addition to that, occurrence of light-induced structural reorganisation of the purple bacteria photosynthetic membranes is suggested by the increase of light scattering.

Acknowledgements The work was supported by grants GACR 206/06/0364, GAAV A608170603 and institutional support AV0Z505 10513, MSM6007665808 and MSM6007665801.

References

Amesz J, Neerken S (2002) Excitation energy transfer in anoxygenic photosynthetic bacteria. Photosynth Res 73:73–81. doi:10.1023/A:1020425030675

Bernhardt K, Trissl H-W (2000) Escape probability and trapping mechanism in purple bacteria: revisited. Biochim Biophys Acta 1457:1–17. doi:10.1016/S0005-2728(99)00103-6

Bina D, Litvin R, Vacha F, Siffel P (2006) New multichannel kinetic spectrophotometer-fluorimeter with pulsed measuring beam for photosynthesis research. Photosynth Res 88:351–356. doi:10.1007/s11120-006-9071-y

Bulychev AA, Niyazova MM, Turovetsky VB (1986) Electro-induced changes of chlorophyll fluorescence in individual intact chloroplasts. Biochim Biophys Acta 810:218–225

Comayras R, Jungas C, Lavergne J (2005a) Functional consequences of the organization of the photosynthetic apparatus in *Rhodobacter sphaeroides*-I. Quinone domains and excitation transfer in chromatophores and reaction center·antenna complexes. J Biol Chem 280:11203–11213. doi:10.1074/jbc.M412088200

Comayras R, Jungas C, Lavergne J (2005b) Functional consequences of the organization of the photosynthetic apparatus in *Rhodobacter sphaeroides*-II. A study of PufX(-) membranes. J Biol Chem 280:11214–11223. doi:10.1074/jbc.M412089200

Cotton NPL, Jackson JB (1982) The kinetics of carotenoid absorption changes in intact cells of photosynthetic bacteria. Biochim Biophys Acta 679:138–145. doi:10.1016/0005-2728(82)90265-1

Dau H, Sauer K (1991) Electric field effect on chlorophyll fluorescence and its relation to Photosystem II charge separation reactions studied by a salt jump technique. Biochim Biophys Acta 1098:49–60. doi:10.1016/0005-2728(91)90008-C

Dau H, Windecker R, Hansen U-P (1991) Effect of light-induced changes in thylakoid voltage on chlorophyll fluorescence of *Aegopodium podagraria* leaves. Biochim Biophys Acta, 337–345

Drews G, Golecki JR (1995) Structure, molecular organization, and biosynthesis of membranes of purple bacteria. In: Blankenship RE, Madigan MT, Bauer CE (eds) Anoxygenic photosynthetic bacteria. Kluwer Academic Publishers, Dordrecht, pp 231–257

Franzen S, Stanley RJ (2002) A theoretical explanation for quantum yield failure in bacterial photosynthetic reaction centers. Chem Phys 276:115–127. doi:10.1016/S0301-0104(01)00582-1

Ghosh R, Tschopp P, Ghosh-Eicher S, Bachofen R (1994) Protein phosphorylation in *Rhodospirillum rubrum*: further characterization of the B873 kinase activity. Biochim Biophys Acta 1184:37–44. doi:10.1016/0005-2728(94)90151-1

Gottfried DS, Stocker JW, Boxer SG (1991) Stark effect spectroscopy of bacteriochlorophyll in light-harvesting complexes from photosynthetic bacteria. Biochim Biophys Acta 1059:63–75. doi:10.1016/S0005-2728(05)80188-4

Grammel H, Ghosh R (2008) Redox-state dynamics of ubiquinone-10 imply cooperative regulation of photosynthetic membrane expression. J Bacteriol 190:4912–4921. doi:10.1128/JB.00423-08

de Grooth BG, Amesz J (1977) Electrochromic absorbance changes of photosynthetic pigments in *Rhodopseudomonas sphaeroides*. Biochim Biophys Acta 462:237–246. doi:10.1016/0005-2728(77)90122-0

Holmes NG, Allen JF (1986) Protein posphorylation as a control for excitation energy transfer in *Rhodospirillum rubrum*. FEBS Lett 200:144–148. doi:10.1016/0014-5793(86)80527-0

Jackson JB, Crofts AR (1969) The high energy state in chromatophores from *Rhodopseudomonas sphaeroides*. FEBS Lett 4:185–189. doi:10.1016/0014-5793(69)80230-9

Joliot P, Verméglio A, Joliot A (1989) Evidence for supercomplexes between reaction centers, cytochrome c_2 and cytochrome bc_1 complex in *Rhodobacter sphaeroides* whole cells. Biochim Biophys Acta 975:336–345. doi:10.1016/S0005-2728(89)80341-X

Joliot P, Joliot A, Verméglio A (1997) Photo-induced cyclic electron transfer operates in frozen cells of *Rhodobacter sphaeroides*. Biochim Biophys Acta 1318:374–384. doi:10.1016/S0005-2728(96)00114-4

Joliot P, Joliot A, Vermeglio A (2005) Fast oxidation of the primary electron acceptor under anaerobic conditions requires the organization of the photosynthetic chain of *Rhodobacter sphaeroides* in supercomplexes. Biochim Biophys Acta 1706:204–214. doi:10.1016/j.bbabio.2004.11.002

Joss A, Mez K, Känel B, Hanselmann KW, Bachofen R (1994) Measurement of fluorescence kinetics of phototrophic bacteria in the natural environment. J Plant Physiol 144:333–338

Jungas C, Ranck JL, Rigaud JL, Joliot P, Verméglio A (1999) Supramolecular organization of the photosynthetic apparatus of *Rhodobacter sphaeroides*. EMBO J 18:534–542. doi:10.1093/emboj/18.3.534

Kingma H, Duysens LNM, Van Grondelle R (1983) Magnetic field-stimulated luminiscence and a matrix model for energy transfer. A new method for determining the redox state of the first quinone acceptor in the reaction center of whole cells of *Rhodospirillum rubrum*. Biochim Biophys Acta 725:434–443. doi:10.1016/0005-2728(83)90184-6

Koblizek M, Shih JD, Breitbart SI, Ratcliffe EC, Kolber ZS, Hunter CN, Niederman RA (2005) Sequential assembly of photosynthetic units in *Rhodobacter sphaeroides* as revealed by fast repetition rate analysis of variable bacteriochlorophyll a fluorescence. Biochim Biophys Acta 1706:220–231. doi:10.1016/j.bbabio.2004.11.004

Kolber ZS, Plumley FG, Lang AS, Beatty JT, Blankenship RE, Van Dover CL, Vetriani C, Koblizek M, Rathgeber C, Falkowski PG (2001) Contribution of aerobic photoheterotrophic bacteria to the carbon cycle in the ocean. Science 292:2492–2495. doi:10.1126/science.1059707

Kramer DM, Sacksteder CA (1998) A diffused-optics flash kinetic spectrophotometer (DOFS) for measurements of absorbance changes in intact plants in the steady-state. Photosynth Res 56:103–112. doi:10.1023/A:1005968211506

Lao K, Franzen S, Stanley RJ, Lambright DJ, Boxer SG (1993) Effect of applied electric fields on the quantum yeld of the initial electron-transfer steps in bacterial photosynthesis. I. Quantum yield failure. J Phys Chem B 97:13165–13171. doi:10.1021/j100152a022

Lao K, Franzen S, Steffen M, Lambright D, Stanley R, Boxer SG (1995) Effect of applied electric fields on the quantum yields for the initial electron transfer steps in bacterial photosynthesis. II. Dynamic Stark effect. Chem Phys 197:259–275. doi:10.1016/0301-0104(95)00090-B

Lavergne J, Joliot P, Verméglio A (1989) Partial equilibration of photosynthetic electron carriers under weak illumination: a theoretical and experimental study. Biochim Biophys Acta 975:346–354. doi:10.1016/S0005-2728(89)80342-1

Law CJ, Cogdell RJ, Trissl H-W (1997) Antenna organisation in the purple bacterium *Rhodopseudomonas acidophila* studied by fluorescence induction. Photosynth Res 52:157–165. doi:10.1023/A:1005853617251

Mulkidjanian AY, Junge W (1994) Calibration and time resolution of lumenal pH-transients in chromatophores of *Rhodobacter capsulatus* following a single-turnover flash of light: proton release by the cytochrome bc_1-complex is strongly electrogenic. FEBS Lett 353:189–193. doi:10.1016/0014-5793(94)01031-5

Okamura MY, Feher G, Nelson N (1982) Reaction centers. In: Govindjee (ed) Photosynthesis: energy conversion by plants and bacteria, vol 1. Academic Press, NY, pp 195–272

Popovic ZD, Kovacs GJ, Vincett PS, Alegria G, Dutton PL (1986) Electric-field dependence of the quantum yield in reaction centers of photosynthetic bacteria. Biochim Biophys Acta 851:38–48. doi:10.1016/0005-2728(86)90246-X

Pospisil P, Dau H (2002) Valinomycin sensitivity proves that light-induced thylakoid voltages result in millisecond phase of chlorophyll fluorescence transients. Biochim Biophys Acta 1554:94–100. doi:10.1016/S0005-2728(02)00216-5

Schmidt KA, Trissl HW (1998) Combined fluorescence and photovoltage studies on chlorosome containing bacteria I. Whole cells of Chloroflexus aurantiacus. Photosynth Res 58:43–55. doi:10.1023/A:1006045711794

Setlik I, Waldburger-Schlapp M, Bachofen R (1990) Slow fluorescence transients in photosynthetic bacteria. In: Baltscheffsky M (ed) Current research in photosynthesis. Kluwer Academic Publishers, Dordrecht, pp 341–344

Sherman LA, Cohen WS (1972) Proton uptake and quenching of bacteriochlorophyll fluorescence in *Rhodopseudomonas spheroides*. Biochim Biophys Acta 283:54–66. doi:10.1016/0005-2728(72)90098-9

Siefert E, Irgens RL, Pfennig N (1978) Phototrophic purple and green bacteria in a sewage treatment plant. Appl Environ Microbiol 35:38–44

Sistrom WR (1962) The kinetics of the synthesis of photopigments in *Rhodopseudomonas sphaeroides*. J Gen Microbiol 28:607–616

Steiger J, Sauer K (1995) Electric field effects on the steady-state fluorescence emission of *Rb. sphaeroides* chromatophores. In: Mathis M (ed) Photosynthesis: from light to biosphere. Kluwer Academic Publishers, Dordrecht, pp 735–738

Strasser RJ, Ghosh R (1995) The fast fluorescence transient of *Rhodospirillum rubrum* is polyphasic of the type O-K-J-I-P. In: Mathis M (ed) Photosynthesis: from light to biosphere. Kluwer Academic Publishers, Dordrecht, pp 915–918

Sturgis JN, Niederman RA (2008) Atomic force microscopy reveals multiple patterns of antenna organization in purple bacteria: implications for energy transduction mechanisms and membrane modeling. Photosynth Res 95:269–278. doi:10.1007/s11120-007-9239-0

Tanaka S, Marcus RA (1997) Electron transfer model for the electric field effect on quantum yield of charge separation in bacterial photosynthetic reaction centers. J Phys Chem B 101:5031–5045. doi:10.1021/jp9632854

Trissl H-W (1996) Antenna organisation in purple bacteria investigated by means of fluorescence induction curves. Photosynth Res 47:175–185. doi:10.1007/BF00016180

Trissl H-W, Law CJ, Cogdell RJ (1999) Uphill energy transfer in LH2-containing purple bacteria at room temperature. Biochim Biophys Acta 1412:149–172. doi:10.1016/S0005-2728(99)00056-0

van Grondelle R (1985) Excitation energy transfer, trapping and annihilation in photosynthetic systems. Biochim Biophys Acta 811:147–195

van Grondelle R, Dekker JP, Gillbro T, Sundström V (1994) Energy transfer and trapping in photosynthesis. Biochim Biophys Acta 1187:1–65. doi:10.1016/0005-2728(94)90166-X

Varga AR, Staehelin LA (1985) Membrane adhesion in photosynthetic bacterial-membranes-light harvesting complex-I (LhI) appears to be the main adhesion factor. Arch Microbiol 141:290–296. doi:10.1007/BF00428839

Verméglio A, Joliot P (2002) Supramolecular organisation of the photosynthetic chain in anoxygenic bacteria. Biochim Biophys Acta 1555:60–64. doi:10.1016/S0005-2728(02)00255-4

Vredenberg WJ (2000) A three-state model for energy trapping and chlorophyll fluorescence in photosystem II incorporating radical pair recombination. Biophys J 79:26–38. doi:10.1016/S0006-3495(00)76271-0

Vredenberg WJ, Bulychev AA (2002) Photo-electrochemical control of photosystem II chlorophyll fluorescence in vivo. Bioelectrochemistry 57:123–128. doi:10.1016/S1567-5394(02)00062-2

Vredenberg WJ, Bulychev AA (2003) Photoelectric effects on chlorophyll fluorescence of photosystem II in vivo. Kinetics in the absence and presence of valinomycin. Bioelectrochemistry 60:87–95. doi:10.1016/S1567-5394(03)00053-7